

Catalysis Science & Technology

Accepted Manuscript



This article can be cited before page numbers have been issued, to do this please use: S. Pang, Y. Zhang, Y. Huang, H. Yuan and F. Shi, *Catal. Sci. Technol.*, 2017, DOI: 10.1039/C7CY00231A.



This is an Accepted Manuscript, which has been through the Royal Society of Chemistry peer review process and has been accepted for publication.

Accepted Manuscripts are published online shortly after acceptance, before technical editing, formatting and proof reading. Using this free service, authors can make their results available to the community, in citable form, before we publish the edited article. We will replace this Accepted Manuscript with the edited and formatted Advance Article as soon as it is available.

You can find more information about Accepted Manuscripts in the [author guidelines](#).

Please note that technical editing may introduce minor changes to the text and/or graphics, which may alter content. The journal's standard [Terms & Conditions](#) and the ethical guidelines, outlined in our [author and reviewer resource centre](#), still apply. In no event shall the Royal Society of Chemistry be held responsible for any errors or omissions in this Accepted Manuscript or any consequences arising from the use of any information it contains.



Journal Name

ARTICLE

N/O-Doped Carbon as “Solid Ligand” for Nano-Pd Catalyzed Biphenyl- and Triphenylamine Synthesis

Shaofeng Pang,^{a,b} Yujing Zhang,^{a,b} Yongji Huang,^a Hangkong Yuan^a and Feng Shi^{*a}Received 00th January 20xx,
Accepted 00th January 20xx

DOI: 10.1039/x0xx00000x

www.rsc.org/

A series of N/O-doped porous carbon supported nanopalladium catalysts have been successfully prepared, in which the N/O doped carbons were controllably produced via polypyrrole/furan synthesis and followed by carbonization. These catalysts exhibit nice performance in biphenylamine and triphenylamine synthesis with nitrobenzene and cyclohexanone as starting materials. Their catalytic activity can be tuned efficiently by the N/O functional groups on the carbon surface. TEM, XRD, XPS and Laser Raman methods were applied to probe the structure of these catalysts. These results indicate that the Pd nanoparticles were supported on N/O-doped porous carbon via the “coordination” between Pd nanoparticles and N/O functional groups including O-C=O, C=N and tertiary nitrogen, and better catalytic performance was obtained if carbon with the highest N-species loading was used as support. In addition, mechanistic study proves that the reaction starts with the catalytic reduction of nitrobenzene with cyclohexanone as the hydrogen source. During this reaction, aniline was formed and the cyclohexanone was transformed into phenol. Then biphenylamine and triphenylamine were generated through the reaction of aniline and cyclohexanone. This work should facilitate the controllable preparation of carbon supported nanocatalysts with specific activity, and open up a promising pathway for the development of new methodologies for N-containing fine chemical synthesis.

1. INTRODUCTION

The controllable preparation of heterogeneous catalyst from molecular level has been intensively pursued by chemists,¹⁻¹¹ while it is difficult to be achieved due to the complicated structure of traditional inorganic supports. Nano-carbon materials with well-defined molecular structures, including amorphous carbon, ordered mesoporous carbon, graphite/graphene (oxide) and carbon nanotubes, etc.,¹²⁻¹⁶ are widely applied in catalytic transformations.¹⁷⁻²⁵ It might present a promising way to design and prepare nano-carbon materials with molecularly defined structure containing specific elements or functional groups, which can adjust the properties of the carbon materials as supports. Among them, N/O-doped nano-carbon materials can be regarded as N/O-substituted graphite and becomes a promising source for the production of free-standing nitrogen or oxygen-rich carbon materials.²⁶⁻³⁰ As it is well known, the N- and O-functional groups play key roles in homogeneous catalysis and they can strongly influence the catalytic efficiency in specific reactions.³¹⁻⁴⁰ Over a long time, more works have been

focused on the exploitation and development of active heterogeneous catalysis systems to integrate the high activity of homogeneous catalysis and easy separability of heterogeneous catalysis.⁴¹⁻⁴⁸ Unfortunately, it remains a challenge in catalysis study. Inspired by the discussions above, the development of controllable preparation of carbon supports with different N/O functional groups⁴⁹⁻⁵⁶ might present a potential to build heterogeneous catalysts with comparable activity to homogeneous catalysts,⁵⁷⁻⁶⁰ because N-⁶¹⁻⁶⁸ or O-^{69, 70}containing ligands are widely used in homogeneous reactions such as palladium-catalyzed dehydrogenation or hydrogenation reactions.

Polypyrrole is an extensively studied polymer that possesses high nitrogen content and leaves a high amount of carbonaceous residue after pyrolysis (yield \approx 60 wt%),⁷¹⁻⁷⁴ which then leads to an effective way for N-doped carbon materials preparation. Nevertheless, to the best of our knowledge, polyfuran has been less extensively studied. Oxypolymerization is an efficient way in mixing-polymerization of pyrrole and furan,⁷⁵⁻⁷⁹ and N,O-rich carbons with tunable N/O ratios can be obtained followed by carbonization, which can be used as “solid ligand” to instead of N/O-containing ligands in catalysts. In this way, a heterogeneous catalysis system with high activity and selectivity for specific reaction might be established. In addition, the proportion of N and O functional groups of the final solid carbons can be adjusted by changing the ratios of pyrrole and furan in the initial stage. If nano-palladium particles were further supported on the “solid ligand”, heterogeneous catalyst with specific activities might be achieved. In this work, a series of carbon materials with different N/O ratios were prepared as support or “solid ligand”

^a State Key Laboratory for Oxo Synthesis and Selective Oxidation, Centre for Green Chemistry and Catalysis, Lanzhou Institute of Chemical Physics, Chinese Academy of Sciences, No. 18, Tianshui Middle Road, Lanzhou, P. R. China.
E-mail: fshi@licp.cas.cn.

^b University of Chinese Academy of Sciences, Beijing, 100049.

Electronic Supplementary Information (ESI) available: [details of any supplementary information available should be included here]. See DOI: 10.1039/x0xx00000x

Journal Name

ARTICLE



Scheme 1. Preparation of Pd/C-py, Pd/C-py/fu and Pd/C-fu through the palladium nanoparticles supported on functionalized porous carbons

for nanopalladium, which were denoted as Pd/C-py, Pd/C-py/fu and Pd/C-fu, respectively (**Scheme 1**).

Arylamines, especially biphenyl- and triphenylamine, are considerable importance in a variety of industrial processes, so the development of simple and economic methods for their preparation is of significant interest. In addition, the introduction of functional groups with specific patterns around the aromatic rings of arylamines is at the forefront of fine chemical synthesis, and it entails a strong potential for industrial developments. Among the methodologies for arylamines synthesis,^{80, 81} the reaction of nitrobenzene and cyclohexanone, which involves the aniline generation via hydrogen transferring from cyclohexanone to nitrobenzene and followed by the coupling reaction of aniline and cyclohexanone, can be a good choice for the controllable synthesis of diphenylamine and triphenylamine. So it was chosen as the model reaction to test the catalytic performance of the “solid ligand” supported nanopalladium catalysts.

2. EXPERIMENTAL SECTION

Typical procedure for C-py preparation⁷¹⁻⁷⁴: 6 g pyrrole was added to a solution of FeCl₃·6H₂O (0.5 M, 400 mL) and the mixture was magnetically stirred for 2 h to synthesize polypyrrole. The polypyrrole was then separated by filtration and washed with deionized water/methanol ($V_{\text{water}} : V_{\text{methanol}} = 1 : 1$) and HCl (10 wt%). The polypyrrole was then dried in air at 80 °C. The final polypyrrole yield was about 100%. The polypyrrole was chemically activated by heating a polypyrrole-KOH mixture (polypyrrole/KOH = 2, w/w) under N₂ flow (99.999%) at 600 °C for 1 h (heating rate: 3 °C·min⁻¹). Finally, the reactor was cooled to room temperature under the N₂ flow, and C-py was obtained. The sample was then thoroughly

washed for several times with HCl (10 wt%) to remove the inorganic salts and then washed with deionized water. Finally, the activated carbon was dried in air at 120 °C and 2.1 g carbon material was produced with a carbonization ratio of 35%.

Typical procedure for C-fu preparation: 6 g furan was added to a chloroform solution of FeCl₃ (0.5 M, 400 mL) and the mixture was magnetically stirred for 24 h to synthesize polyfuran. The polyfuran was then separated by filtration and washed with chloroform/methanol solution ($V_{\text{chloroform}} : V_{\text{methanol}} = 1 : 1$) and HCl (10 wt%). The polyfuran was dried in air at 80 °C, and the polyfuran yield was about 100%. Following, the polyfuran was activated by heating a polyfuran-KOH mixture (KOH/Polypyrrole = 2, w/w) under N₂ (99.999%) at 600 °C for 1 h (heating rate: 3 °C·min⁻¹). Finally, the reactor was cooled to room temperature under the N₂ flow, and C-py was obtained. The sample was then thoroughly washed for several times with HCl (10 wt%) to remove the inorganic salts and then washed with deionized water. Finally, the activated carbon was dried in air at 120 °C and 1.8 g carbon material was produced with a carbonization ratio of 30%.

Typical procedure for C-py/fu-3 preparation: A mixture of 4.5 g pyrrole and 4.5 g furan was added to a chloroform solution of FeCl₃ (0.5 M, 400 mL) and the mixture was magnetically stirred for 24 h to synthesize polypyrrole/furan. The polymer was then separated by filtration and washed with chloroform/methanol solution ($V_{\text{chloroform}} : V_{\text{methanol}} = 1 : 1$) and HCl (10 wt%). The polymer was dried in air at 80 °C and the polymer yield was about 100%. The polymer was activated by heating a polymer-KOH mixture (KOH/Polymer = 2, w/w) under N₂ (99.999%) at 600 °C for 1 h (heating rate: 3 °C·min⁻¹). Finally, the reactor was cooled to room temperature under the

N₂ flow, and C-py was obtained. The sample was then thoroughly washed for several times with HCl (10 wt%) to remove the inorganic salts and then washed with deionized water. Finally, the activated carbon was dried in air at 120 °C and 2.1 g carbon material was produced with a carbonization ratio of 35%.

Typical procedure for carbon supported nanocatalysts preparation: 0.7 g carbon and 240 mL deionized water were mixed in a round-bottom flask and stirred at room temperature for 1 h. Then, 2.1 mL H₂PdCl₄ (0.282 M) was added dropwise and the mixture was further stirred for 4 h. Then 3 mL NaOH (5 M) was added dropwise and the mixture was stirred for 2 h. Following, 14 mL formaldehyde solution (38 wt%) was added as reducing agent at 80 °C. The reaction mixture was stirred overnight, and the catalyst was then separated by filtration, and washed with deionized water and dried in air at 80 °C for 5 h. The catalyst sample was denoted as Pd/C-py/fu-3. Different catalysts were prepared with the same procedure, and denoted as Pd/C-fu, Pd/C-py/fu-1, Pd/C-py/fu-2, Pd/C-py/fu-3, Pd/C-py/fu-4, Pd/C-py, Pd/C-py-x, Pt/C-py and Ru/C-py. Pd/C-py catalyst being used for three runs was denoted as Pd/C-py-R.

Catalyst characterization: Transmission electron microscopy (TEM) characterization was carried out by using a Tecnai G2 F30 S-Twin transmission electron microscope operating at 300 kV. Single-particle EDX analysis was performed by using a Tecnai G2 F30 S-Twin Field Emission TEM in STEM mode. For TEM investigations, the catalysts were dispersed in ethanol by ultrasonication and deposited on carbon-coated copper grids. XRD measurements were conducted by using a STADIP automated transmission diffractometer (STOE) equipped with an incident beam curved germanium monochromator with Cu_{Kα1} radiation. The catalyst samples were dried in air and pressed on a glass slide for analysis. The XRD patterns were scanned in the 2θ range of 10–80°. For data interpretation, the software WinXpov (STOE) and the database of powder diffraction file (PDF) of the International Centre of Diffraction Data (ICDD) were used. The X-ray photoelectron spectroscopy (XPS) measurements were carried out by using a VG ES-CALAB 210 instrument equipped with a dual Mg/Al anode X-ray source, a hemispherical capacitor analyzer, and a 5 keV Ar⁺ ion gun. All spectra were recorded by using nonmonochromatic Mg_{Kα} (1253.6 eV) radiation. The samples were fixed to a stainless steel sample holder by using double-sided adhesive carbon tape. The electron binding energy was referenced to the C_{1s} peak at 284.8 eV. The peaks were fitted by Gaussian–Lorentzian curves after a Shirley background subtraction. For quantitative analysis, the peak area was divided by the element-specific Scofield factor and the transmission function of the analyzer. The background pressure in the chamber was less than 10^{−7} Pa. Raman spectra were measured with 532nm-Edge by using LabRAM HR Evolution (HORIBA Jobin Yvon S.A.S.). Nitrogen adsorption–desorption isotherms were measured at 77 K by using a Quanta chrome autosorb iQ₂ instrument. The pore-size distribution was calculated from the desorption isotherm by using the Barrett, Joyner, and Halenda (BJH) method. The BET surface areas of Pd/C-fu, Pd/C-py/fu-1,

Pd/C-py/fu-2, Pd/C-py/fu-3, Pd/C-py/fu-4, Pd/C-py, Pd/C-py-x, Pt/C-py and Ru/C-py were 745 m²/g, 767 m²/g, 839 m²/g, 906 m²/g, 1128 m²/g, 1571 m²/g, 2602 m²/g, 1446 m²/g and 1870 m²/g. The loadings of all catalyst samples were determined by ICP-AES. The metal loadings of Pd/C-fu, Pd/C-py/fu-1, Pd/C-py/fu-2, Pd/C-py/fu-3, Pd/C-py/fu-4, Pd/C-py, Pd/C-py-x, Pt/C-py and Ru/C-py were 7.4 wt%, 7.6 wt%, 7.3 wt%, 7.5 wt%, 7.4 wt%, 7.4 wt%, 7.3 wt%, 6.7 wt% and 7.1 wt%, respectively. Elemental analysis (N, C, O, and H) of the samples was carried out on a Vario EL microanalyzer. NMR spectra were measured by using a Bruker ARX 400 or ARX 100 spectrometer at 400 MHz (¹H) and 101 MHz (¹³C). All spectra are reported in ppm relative to tetramethylsilane referenced to the residual solvent peaks.

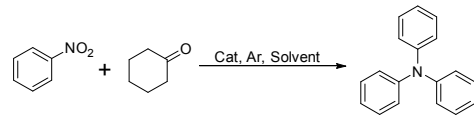
Synthesis of triphenylamine: 0.5 mmol nitrobenzene, 4 mmol cyclohexanone, 30 mg catalyst and 5 mL toluene were added to a 38 mL pressure tube equipped with a magnetic stirrer and reacted at 160 °C for 36 h under Ar. Then the reaction mixture was cooled to room temperature. The crude reaction mixture was concentrated in vacuo and purified by column chromatography to give triphenylamine in 96% isolated yield.

Synthesis of diphenylamine: 0.5 mmol nitrobenzene, 6 mmol cyclohexanone, 100 mg catalyst and 2 mL toluene were added to a 15 mL pressure tube equipped with a magnetic stirrer and reacted at 80 °C for 36 h under Ar. Then the reaction mixture was cooled to room temperature. The crude reaction mixture was concentrated in vacuo and purified by column chromatography to give biphenylamine in 82% isolated yield.

Purification procedure: The crude products were subjected to silica gel column chromatography (60, 230–400 mesh supplied by Qingdao Haiyang Chemical and Special Silica Gel Co, Ltd). Eluting with ~75 mL of Petroleum Ether, followed by 200 : 1 (Petroleum Ether : EtOAc).

3. RESULTS AND DISCUSSION

Performance of the catalysts. As a proof-of-concept application of the “solid ligand” catalyst, such a model reaction could directly reflect the catalytic activity of the activated metal nanoparticles with different ratios of oxygen/nitrogen doped carbon materials. The performance of the prepared catalysts for synthesis of triphenylamine via the reaction of nitrobenzene and cyclohexanone was tested first, as shown in **Table 1**. Obviously, the Pd/C-py exhibits better catalytic performance, and no triphenylamine was observed if Pd/C-fu was used as catalyst (**Table 1, entries 1 and 6**). With the increasing of the mass ratios of pyrrole during polymer synthesis, the catalytic performance can be improved significantly and 99% nitrobenzene conversion with 96% triphenylamine yield were obtained when Pd/C-py was used as the catalyst (**entries 1–6**). Therefore, the presence of nitrogen but not oxygen group is essential to gain high activity. To our delight, the catalyst can be recovered for 3 runs without obvious catalyst activity decreasing (**entry 6**). The Pd loading maintained 7.3 wt% after being used for three runs. It is almost the same as the fresh catalyst, which is 7.4 wt%, suggesting no palladium leaching occurred during the reaction.

Table 1. Results of catalyst screening and reaction conditions optimization.^a


Entry	Catalyst	Py/Fu ^b	Sel. % ^c	Con. % ^d	Y. % ^e
1	Pd/C-fu	0:1	--	26	--
2	Pd/C-py/fu-1	1:4	4	49	2
3	Pd/C-py/fu-2	2:3	22	75	17
4	Pd/C-py/fu-3	1:1	55	99	55
5	Pd/C-py/fu-4	4:1	67	99	67
6	Pd/C-py	1:0	97/ 93 ^g	99/ 99 ^g	96/ 92 ^g
7	Pd/C-py-x ^f	1:0	79	99	78
8	Pt/C-py	1:0	--	--	--
9	Ru/C-py	1:0	--	--	--
10	Pd	--	--	--	--
11	PdO	--	--	--	--
12	Pd/XC-72R	--	--	17	--

^a0.5 mmol nitrobenzene, 4 mmol cyclohexanone, 30 mg catalyst, 5 mL toluene, 160 °C (reaction temperature), 36 h, Ar. ^bthe mass ratios of pyrrole and furan for carbon materials preparation. ^cBET surface area (m²/g). ^dNitrobenzene conversion determined by GC-MS. ^eIsolated yield. ^fPyrolyzed at 700 °C. ^gThe catalyst was used at the 3rd run.

Thus the N-rich carbon from polypyrrole exhibits the best performance as “solid ligand” to support nano-palladium in triphenylamine synthesis from nitrobenzene and cyclohexanone. In addition, Pt/C-py and Ru/C-py were prepared with the same procedures and were used as the catalysts under the same reaction conditions but no reaction was observed (**entries 8-9**). So palladium is the suitable active species in this reaction. As control reactions, the activity of PdO and Pd powder (APS 0.25-0.55 micron) were tested under the same reaction conditions (**entries 10-11**), and no reaction was observed, too. Thus, PdO and Pd powder can not be used as catalyst directly. Noteworthy, the better catalytic performance of Pd/C-py should not be attributed to its higher BET surface area, which was 1571 m²/g, because only 78% triphenylamine yield was obtained if Pd/C-py-x was used as the catalyst, which BET surface area was 2602 m²/g (**entries 6-7**). In consideration of the EA analysis results of different catalysts (**Table 2**), it can be imagined that the presence of suitable amount of N/O groups should be the key factor for the high activity. Finally, Pd/XC-72R was prepared with a commercial active carbon (XC-72R) as support. However, only small amount of biphenylamine was generated and almost no triphenylamine was observed when Pd/XC-72R was used as the catalyst. It can be imagined that the presence of N-groups on porous carbons is essential to gain the high activity. The N-groups might behave as the ligand to modulate the activity of nano-palladium.

Table 2. EA analysis results of different catalysts.^a

Entry	Catalyst	N	C	O	H
1	Pd/C-fu	0.16	70.34	19.42	1.52
2	Pd/C-py/fu-1	2.15	64.51	23.31	1.55
3	Pd/C-py/fu-2	3.78	62.42	24.11	1.71
4	Pd/C-py/fu-3	3.96	59.02	25.87	1.87
5	Pd/C-py/fu-4	4.85	52.77	30.89	2.25
6	Pd/C-py-x	5.03	66.41	18.21	1.48
7	Pd/C-py	8.23	62.25	18.14	2.21
8	Pt/C-py	8.01	70.92	9.37	2.53
9	Ru/C-py	8.72	69.72	9.71	2.61

^aElemental analysis (N, C, O, and H, wt%) of the samples was carried out on a Vario EL microanalyzer.

Catalyst characterizations. In order to reveal the relationship between the catalyst structure and catalytic performance, these catalysts were further characterized by TEM, XRD, XPS and Laser Raman. First, the morphologies and microstructures of the catalysts were examined by TEM, and the images were shown in **Figure 1**.

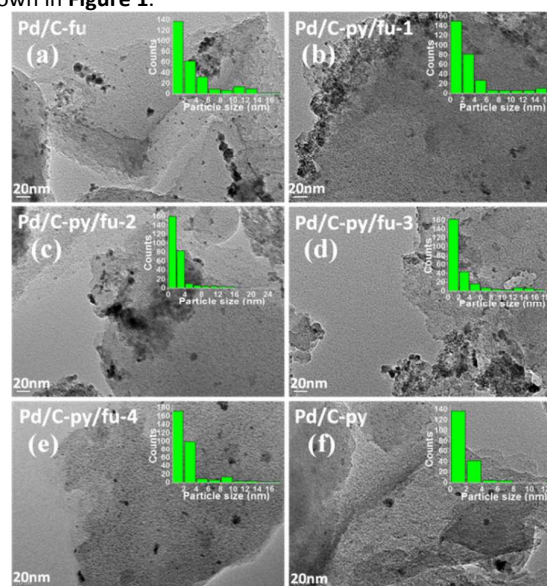


Figure 1. TEM images of Pd/C-fu (a), Pd/C-py/fu-1 (b), Pd/C-py/fu-2 (c), Pd/C-py/fu-3 (d), Pd/C-py/fu-4 (e) and Pd/C-py (f). The insets are the corresponding PSD histograms.

It can be seen clearly that the Pd nanoparticles are well dispersed on the surface of these porous carbon supports, and no obvious Pd nanoparticles aggregation can be observed. Statistical analysis of particle size distribution (PSD) was carried out by measuring the number of Pd nanoparticles on the picture (**insets of Figure 1**). The average Pd diameters of Pd/C-fu, Pd/C-py/fu-1, Pd/C-py/fu-2, Pd/C-py/fu-3, Pd/C-py/fu-4, Pd/C-py and Pd/C-py-R were 3.93 nm, 3.51 nm, 2.89 nm, 2.83 nm, 2.8 nm, 2.3 nm and 2.3 nm, respectively. A more detailed analysis on PSD reveals that with the increase of nitrogen content of supports, the proportion of Pd nanoparticles sizes within 1-4 nm increased (from 72% to 92%). It may be indicated that a stronger metal-support interaction (SMSI) between Pd nanoparticles and the nitrogen functional groups compared to oxygen functional groups.

Energy dispersive X-ray spectroscopy (EDX) elemental line scans over different catalysts (Figure S2) illustrate that the well-distribution of O, N, and Pd in different samples. On the other hand, high-resolution TEM (HR-TEM) images of these catalysts were shown in Figure S3, and the crystal lattice plane distance of Pd(111) (0.245 nm) and Pd(200) (0.194 nm) were observed, which are consistent with the XRD diffraction patterns of the catalyst (Figure 2).

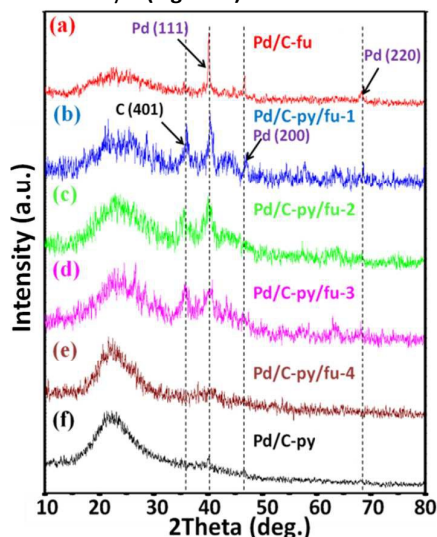


Figure 2. XRD diffraction patterns of Pd/C-fu (a), Pd/C-py/fu-1 (b), Pd/C-py/fu-2 (c), Pd/C-py/fu-3 (d), Pd/C-py/fu-4 (e) and Pd/C-py (f).

More information can be gained from the XRD characterization results. Sharp diffraction peaks of Pd/C-fu centered at 36.025° , 40.118° , 46.658° and 68.119° associated with the C (401), Pd (111), Pd(200) and Pd(220) can be observed (Figure 2a). Interestingly, these diffraction peaks turned weaker with the increasing of nitrogen content in the supports, and no obvious diffraction peaks assigned to Pd nanoparticles can be observed from Pd/C-py. These results suggest that the increasing of N-groups on the carbon supports can influence the morphology of palladium nanoparticles significantly. These results were further confirmed by the selected area electron diffraction (SAED) patterns. In local regions, the Pd/C-fu showed diffraction rings of porous carbons with diffraction spots assigned to the diffraction patterns of Pd (111), Pd(200) and Pd(220), and the Pd/C-py/fu-1 with the diffraction patterns of Pd(111) and Pd(220) (Figure S4). However, there are no diffraction spots regarding crystal Pd nanoparticles from Pd/C-py/fu-2, Pd/C-py/fu-3, Pd/C-py/fu-4 and Pd/C-py can be observed, illustrating ultra-small Pd nanoparticles with low crystallinity on the porous carbons with the increasing of nitrogen content of the supports. Based on aforementioned TEM, EDX, HR-TEM, XRD, and SAED analyses, it further suggested that Pd nanoparticles have a strong interaction with nitrogen functional groups compared with oxygen functional groups. Finally, based on the TEM, HR-TEM and XRD characterization results of Pd/C-py-R, it can be seen that the catalyst structure is not changed remarkably, which

indicates the stability of the catalyst during reaction (Figure S6).

Typical XPS survey scans of the catalysts were shown in Figure S5, revealing that catalyst Pd/C-fu contains C, O and Pd as the main elements and N/O-doped porous carbons catalysts also contains N element. O1s spectra of these series of O-doped, N/O-doped carbon materials and catalysts demonstrate the binding energy of oxygen functional groups, i.e., 532 eV, 532.6 eV and 533.8 eV in C-fu, C-py/fu-3 and C-py (Figure 3a-c). The binding energy of 532 eV is assigned to the oxygen in carboxylate (COO⁻). The binding energy of 532.6 eV is attributed to hydroxyl group (C-OH) of alcohol, phenol, aliphatic ether and carbonyl group (C=O). The binding energy of 533.8 eV demonstrates oxygen of aryl ethers or carboxylic acids (O=C-O). For O1s spectra of the catalysts, the binding energy of 535 eV is related to chemisorbed oxygen in carboxylic groups or water (H-O-H).⁸²⁻⁸⁴ Interestingly, no obvious O1s binding energy shift can be seen in O-doped, N/O-doped carbon materials along with the increasing of nitrogen content, indicating the increase of nitrogen functional groups had no effect on oxygen functional groups by thermal treatment. Whereas, the peak at 532 eV shifts to 531.6 eV, when O-doped and N/O-doped carbon materials are introduced with the palladium nanoparticles (Figure 3d-i). This shift indicates an increase of electron density of the O atoms by the charge transfer from Pd species to O-C=O group. Meanwhile, it is noted that no shift of binding energy were observed for the peaks of 532.6 eV and 533.8 eV before and after Pd loading, respectively. The results of O1s spectra suggest that the local electronic structure of O-C=O in carboxylate can be significantly modified by the interaction with a large amount of Pd active ingredient, and other oxygen functional groups may not have obvious interaction with the Pd species.

It is worth mentioning that O1s spectra of Pd/C-py-N (Figure 3j) (without reduction by formaldehyde) is similar with Pd/C-py. This result showed that the reduction process had no effect on the oxygen functional groups that already exist in N/O-doped carbons. N/O-doped porous carbons are always a complicated system because of the coexistence of various N species, and it is still under debate as to which type of nitrogen functionality is responsible for the electronic interaction. Thus, a series of N/O-doped carbon materials and catalysts with different nitrogen content were prepared to investigate the interaction between the N species and Pd nanoparticles (Figure 4). The N species in C-py/fu-3 and C-py are composed by three types of N, which are attributed to the C=N bond appeared at 398.6 eV, the tertiary nitrogen at 400.1 eV among s-triazine rings and graphitic N-oxide at 400.9 eV, respectively.⁸⁵⁻⁸⁷ (Figure 4a-b).

A noticeable shift of the peaks of C=N bond and tertiary nitrogen from 398.6 eV and 400.1 eV to 398.3 eV and 399.8 eV after loading of palladium nanoparticles (Figure 4c-g). Thus, the introduction of Pd specie into the carbon material generates an increased electron density of N specie, indicating an electron-deficient chemical state of Pd nanoparticles. Yet for all that, there is no obvious shift of binding energy in the

Journal Name

ARTICLE

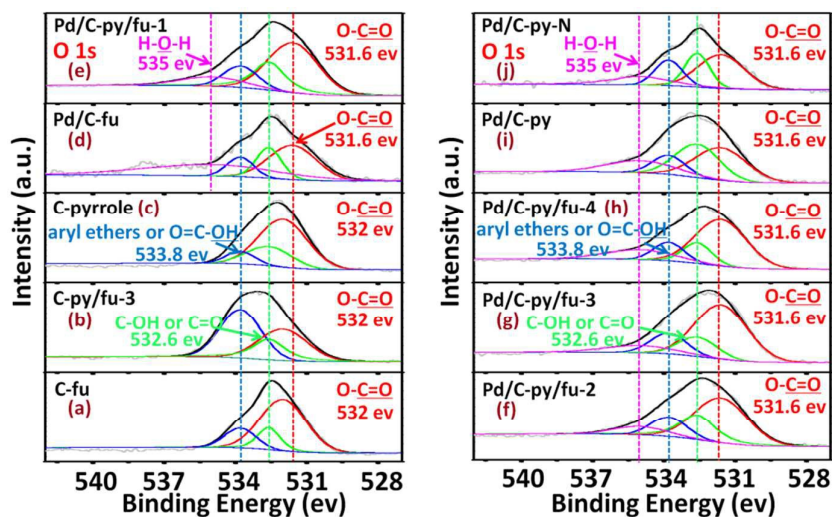


Figure 3. O 1s spectra of C-fu (a), C-py/fu-3 (b), C-py (c), Pd/C-fu (d), Pd/C-py/fu-1 (e), Pd/C-py/fu-2 (f), Pd/C-py/fu-3 (g), Pd/C-py/fu-4 (h), Pd/C-py (i) Pd/C-fu and Pd/C-py without reduction by formaldehyde aqueous solution is labeled as Pd/C-py-N (j)

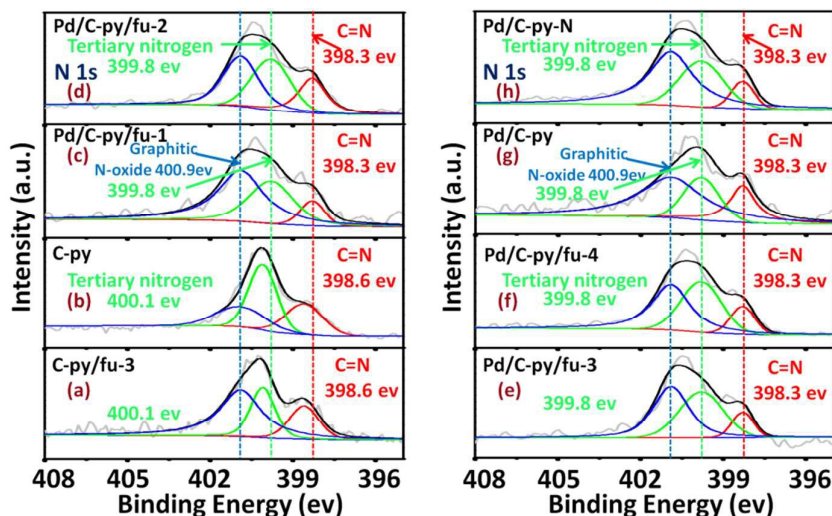


Figure 4. N 1s spectra of C-py/fu-3 (a), C-py (b), Pd/C-py/fu-1 (c), Pd/C-py/fu-2 (d), Pd/C-py/fu-3 (e), Pd/C-py/fu-4 (f), Pd/C-py (g) and Pd/C-py-N (h)

structure of graphitic N-oxide before and after Pd loading. These results may be beyond all expectations, because it is reported that the graphitic N-oxide plays a crucial role in the dehydrogenation and oxygen reduction⁸⁸⁻⁹⁴ due to N-doped graphitic are expected to show stronger π bonds of aromatic rings.⁹⁵⁻⁹⁹ It implies that the electronic interaction is not occurred between graphitic N-oxide and Pd nanoparticles. Accordingly, it can be observed obviously that N1s spectra of Pd/C-py is similar with Pd/C-py-N, indicating the reduction process has absolutely no influence on the existing nitrogen functional groups, too (Figure 4h).

The Pd3d XPS spectra of the catalysts present two peaks at about 335.5 and 340.8 eV, corresponding to the spin-orbit split doublet of Pd3d_{5/2} and 3d_{3/2}, respectively (Figure 5a-f). The Pd3d spectra of Pd/C-fu are de-convoluted into two groups of peaks (Figure 5a), including the predominant metallic Pd and Pd oxide.

The peaks at 335.5 eV (Pd3d_{5/2}) and 340.8 eV (Pd3d_{3/2}) can be attributed to metallic Pd (Peak-1),^{100,101} and peaks at 336.2 eV (Pd3d_{5/2}) and 341.7 eV (Pd3d_{3/2}) can be assigned to the Pd species interacted with the O-C=O groups (Peak-2).¹⁰²

Interestingly, when the N species are introduced into the

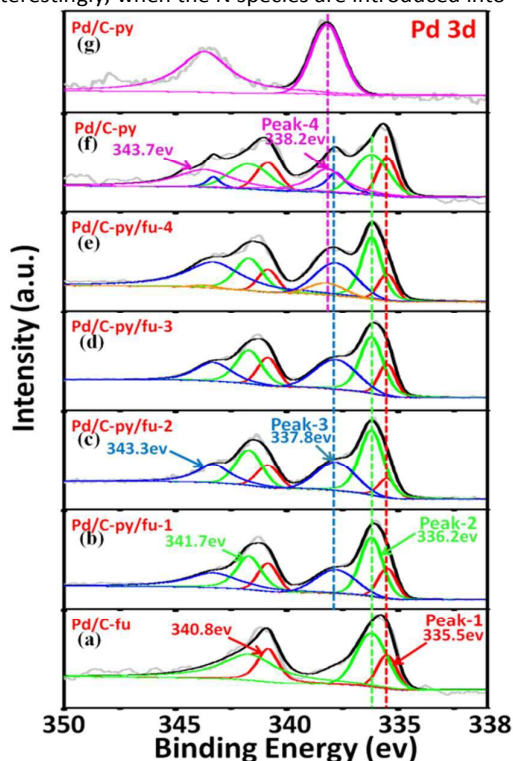


Figure 5. Pd3d spectra of Pd/C-fu (a), Pd/C-py/fu-1 (b), Pd/C-py/fu-2 (c), Pd/C-py/fu-3 (d), Pd/C-py/fu-4 (e), Pd/C-py (f) and Pd/C-py-N (g).

Carbon support, new peaks at 337.8 eV ($\text{Pd}3d_{5/2}$) and 343.3 eV ($\text{Pd}3d_{3/2}$) (Peak-3) can be observed obviously in Pd/C-py/fu-1 and Pd/C-py (Figure 5b-f). In the case of Pd/C-py (Figure 5f), the local electronic structure of Pd nanoparticles can be significantly affected by the interaction with a large amount of nitrogen functional groups, and resulting in Peak-4 with binding energies at 338.2 eV ($\text{Pd}3d_{5/2}$) and 343.7 eV ($\text{Pd}3d_{3/2}$). Whereas, it is also worth pointing out that no shifting with the already existing peaks (peak-1 and peak-2) of Pd 3d binding energy toward the low-energy side can be observed, although nitrogen content is gradually increased from Pd/C-fu to Pd/C-py. Meanwhile, there is no shift of the binding energy of O1s (Figure 3d-i) and N1s (Figure 4c-g), too. In one word, these results suggested that the Pd species might coordinate with the O-C=O groups, C=N and tertiary nitrogen groups,¹⁰³⁻¹⁰⁶ and these functional carbons behave as solid ligands to support palladium nanoparticles. In consideration of the results of the model reaction together (Table 1 entries 1-6), the interaction between the nitrogen functional groups and Pd species might be responsible for the higher activity of Pd/C-py. Also, Pd/C-py-R was characterized by XPS and almost the same O1s, N1s and Pd3d spectra as the fresh Pd/C-py were observed. So the surface structure of the catalyst is stable enough during the reaction (Figure S6).

Raman spectroscopy is a powerful technique to characterize the structures and electronic properties of catalytic materials, particularly to determine the defects, and the ordered and disordered structures of carbon.¹⁰⁷⁻¹⁰⁹ The FT-

Raman spectra of Pd/C-py and Pd/C-fu were given in Figure 6. As for the Pd/C-fu (Figure 6b), two remarkable peaks at 1369 and 1600 cm^{-1} assigned to the well-defined D and G bands can be observed. In the case of Pd/C-py (Figure 6a), broader D band centered at 1363 cm^{-1} is caused by multiple overlapping peaks (the mode of C-N vibration at 1285 cm^{-1} , the mode of C=N at 1400 cm^{-1} and the D mode of graphene),¹⁰⁷⁻¹⁰⁹ whereas the G band centered at 1607 cm^{-1} arises from the overlap of the G bands of graphene.^{110, 111} The high intensity of the D band of Pd/C-py and Pd/C-fu clearly indicates the presence of defects in the carbon material, which should be caused by N/O-doping or O-doping in the porous carbons supports.¹¹² Compared with Pd/C-fu, the ID/IG ratio in Pd/C-py becomes greater, which is not only caused by more disordered structure involving C-N bonds, but also ascribed to the high baseline of Pd/C-py in the region of the D band.

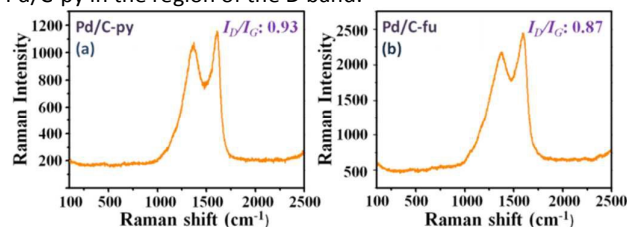
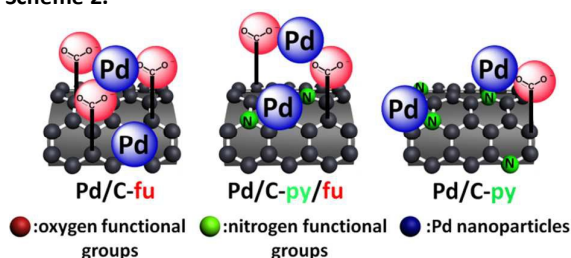


Figure 6. FT-Raman spectra of Pd/C-py (left) and Pd/C-fu (right).

All the above discussions imply both nitrogen functional groups and oxygen functional groups coexisted in porous carbons, so an illustration of the catalyst structures were given in Scheme 2.



Scheme 2. Pictorial description of Pd/C-fu, Pd/C-py/fu and Pd/C-py.

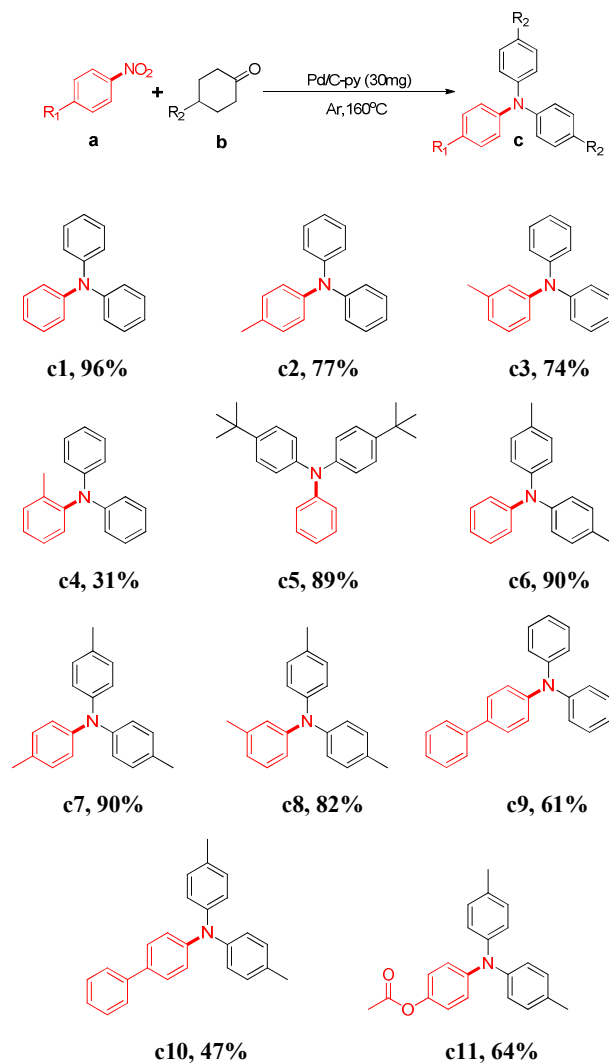
Scope and limitations. It has been reported that palladium-catalyzed synthesis of arylamines from nitrobenzene and cyclohexanone could also be successfully converted to the corresponding substituted diphenylamine at 150 °C with good isolated yields.^{113, 114} However, it is still difficult to synthesize triphenylamine. Therefore, with the optimized reaction conditions in hand, we examined the scope of the reaction with a range of nitrobenzene and cyclohexanone derivatives as starting materials (Scheme 3). The desired triphenylamine derivatives were formed in good yield when nitrobenzene or 4-nitrotoluene was used in combination with cyclohexanone or 4-methylcyclohexanone, and the isolated yields of **c1**, **c6** and **c7** were 96%, 90% and 90%, respectively. The substituting positions on the aromatic ring of nitrobenzene did significantly affect the reaction. The yield of **c4** was only 31% when 2-nitrotoluene and cyclohexanone were used as the starting materials. It needs to be mentioned that the reaction can not progress well if nitrobenzene or cyclohexanone derivatives

ARTICLE

Journal Name

with electron-withdrawing or big substituting groups were used as the starting materials. For example, only 61%, 47% and 64% yields of **c9-11** can be obtained. Even though, this unprecedented sequence offers a synthetically powerful method for the synthesis of triphenylamine derivatives.

Scheme 3. Synthesis of triphenylamine derivatives^a

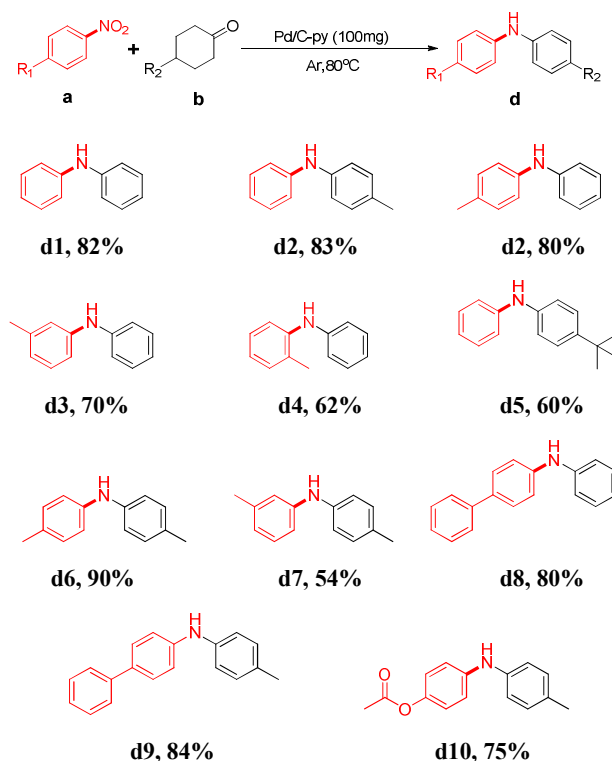


^aIsolated yield.

In order to show the generality of this catalyst system, next, we explore the Pd/C-py-catalyzed synthesis of substituted diphenylamine with nitrobenzene and cyclohexanone derivatives as the starting materials (**Scheme 4**). To our delight, an array of substituted diphenylamine derivatives were obtained with good yields at 80 °C, including products with methyl, *tert*-butyl, phenyl, and ester substituting groups on the aromatic rings (**d1-d10**). The steric-hindered 2-nitrotoluene proceed effectively to 2-methyl-N-phenylaniline (**d4**) in 62% yield, and even the 3-nitrotoluene with 4-methylcyclohexanone affords the corresponding product (**d7**) with 54% yield. Further, the presence of acetate group does

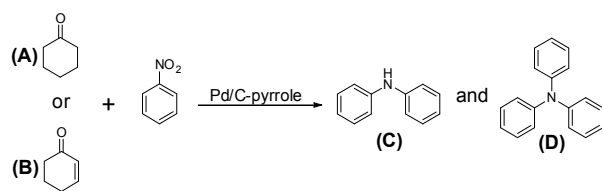
not influence the reactivity of nitrobenzene, and 75% yield of the desired product (**d10**) was obtained.

Scheme 4. Synthesis of diphenylamine derivatives^a



^aIsolated yield.

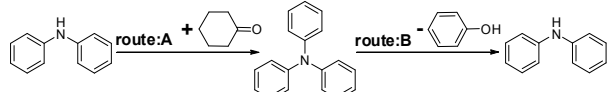
Reaction Mechanism Exploration. In the previous study with aniline and cyclohexanone as starting materials, it has been considered that 2-cyclohexen-1-one may be the possible reaction intermediate.¹¹⁵⁻¹¹⁸ Therefore, in order to get insights into the mechanism of the Pd/C-py catalyzed reaction of nitrobenzene with cyclohexanone to synthesize diphenylamine and triphenylamine, the reaction of nitrobenzene with cyclohexanone or 2-cyclohexen-1-one was carried out with different time intervals (**Table 3**). Clearly, 90% nitrobenzene conversion, 70% diphenylamine yield and 19% triphenylamine obtained at 12 h with cyclohexanone as starting material (**Table 3, entry 1**). If the reaction was extended to 24 h, 14% diphenylamine and 84% triphenylamine yields were obtained (**entry 3**). Finally the yield of triphenylamine reached 96% at 36 h (**entry 5**). If 2-cyclohexen-1-one was used as starting material, 32% biphenylamine and 45% triphenylamine was obtained at 24 h (**entries 2 and 4**), but their yields changed to 53% and 31%, respectively, at 36 h (**entry 6**). Interestingly, 2-cyclohexen-1-one has been consumed, and remarkable amount of cyclohexanone and phenol were generated at 24 h. These results suggested that 2-cyclohexen-1-one should not be the reaction intermediate in this reaction, and it can be transformed into cyclohexanone and phenol in the presence of Pd/C-py catalyst.

Table 3. Control experiments of nitrobenzene and cyclohexanone or 2-cyclohexen-1-one^a

Entry	Reactants	t/h	Con.% ^b	Y(C).% ^c	Y(D).% ^c
1	A	12	90	70	19
2	B	12	99	60	12
3	A	24	99	14	84
4	B	24	99	32	45
5	A	36	99	3	96
6	B	36	99	53	31

^a0.5 mmol nitrobenzene, 4 mmol cyclohexanone (A) or 2-cyclohexen-1-one (B), 30 mg Pd/C-py, 5 mL toluene, 160 °C (reaction temperature), Ar. ^bconversion of nitrobenzene determined by GC-FID with external standard method. ^cGC yields.

In addition, the above results also reveal the reversible transformation between triphenylamine and diphenylamine (Table 3, entries 2, 4 and 6, Scheme 5). Triphenylamine can be formed by reaction of diphenylamine and cyclohexanone (route A), and diphenylamine also can be obtained via the decomposition of triphenylamine with the co-generation of phenol (route B). These results also suggested that the concentration of cyclohexanone is a crucial factor for the Pd/C-py-catalyzed hydrogen transfer reaction. Route A would be the main pathway if the concentration of cyclohexanone is high enough, otherwise triphenylamine can be converted into diphenylamine in this catalytic system.



Scheme 5. Reversible transformation between triphenylamine and diphenylamine

In order to clarify the reaction process, the reaction of nitrobenzene and cyclohexanone was traced by GC-FID to

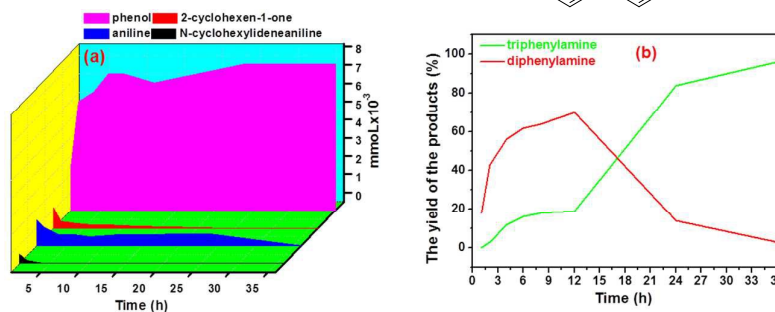
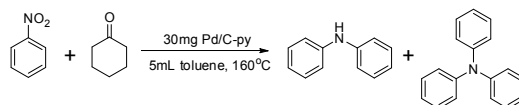
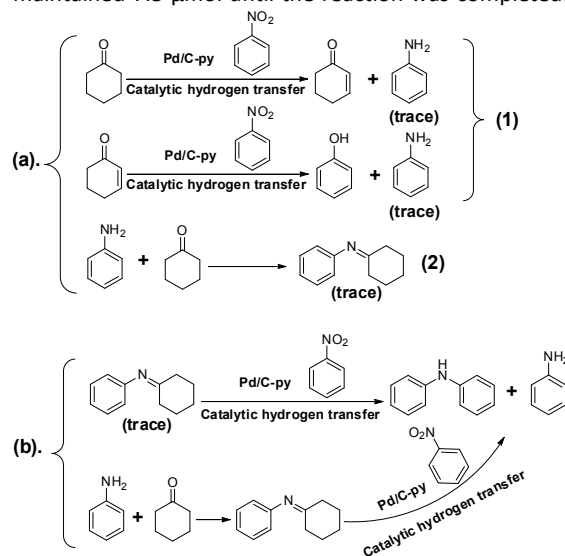


Figure 7. The model reactions with different time intervals (from 1 h to 36 h). The content of starting materials and intermediates determined by GC-FID with external standard method.

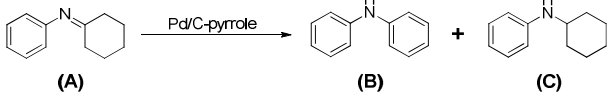
determine the quantities of starting materials and products at different reaction times (Table 1, entry 6, and Figure 7). 1.1 μmol 2-cyclohexen-1-one, 1.4 μmol aniline and 0.5 μmol N-cyclohexylideneaniline were formed in 1 h. Following, the content of 2-cyclohexen-1-one and aniline decreased remarkably at 2 h, i.e., 0.35 μmol 2-cyclohexen-1-one, 1 μmol aniline and 0.175 μmol N-cyclohexylideneaniline can be observed inside the reaction mixture. Meanwhile, the yields of diphenylamine (43%) and triphenylamine (3%) has an obvious increase. Notably, N-cyclohexylideneaniline can not be observed obviously at 5 h, whereas, 0.23 μmol 2-cyclohexen-1-one and 0.6 μmol aniline were still maintained. These result imply that N-cyclohexylideneaniline may be the reaction intermediate. As the reaction continued, the content of 2-cyclohexen-1-one, aniline and N-cyclohexylideneaniline decreased, but the amount of phenol increased slightly, and 7.5 μmol phenol formed at 23 h. The content of phenol has maintained 7.5 μmol until the reaction was completed. These



Scheme 6. process-A (a) and process-B (b) of the catalytic hydrogen transfer processes.

results implicate that the reaction process may be composed of two reaction processes (**Scheme 6**). In the reaction-A (**Scheme 6a**), 2-cyclohexen-1-one and aniline were generated via transfer hydrogenation. Next, 2-cyclohexen-1-one reacted with nitrobenzene to form phenol and aniline. Meanwhile, aniline reacted with cyclohexanone, and N-cyclohexylideneaniline generated for reaction-B (**Scheme 6b**). In addition, the content of phenol maintained unchanged at 7.5 μmol from 23 h to the completion of the reaction. So it was deduced that reaction-A almost stopped when reaction-B started.

Table 4. Catalytic transformation of N-cyclohexylideneaniline^a

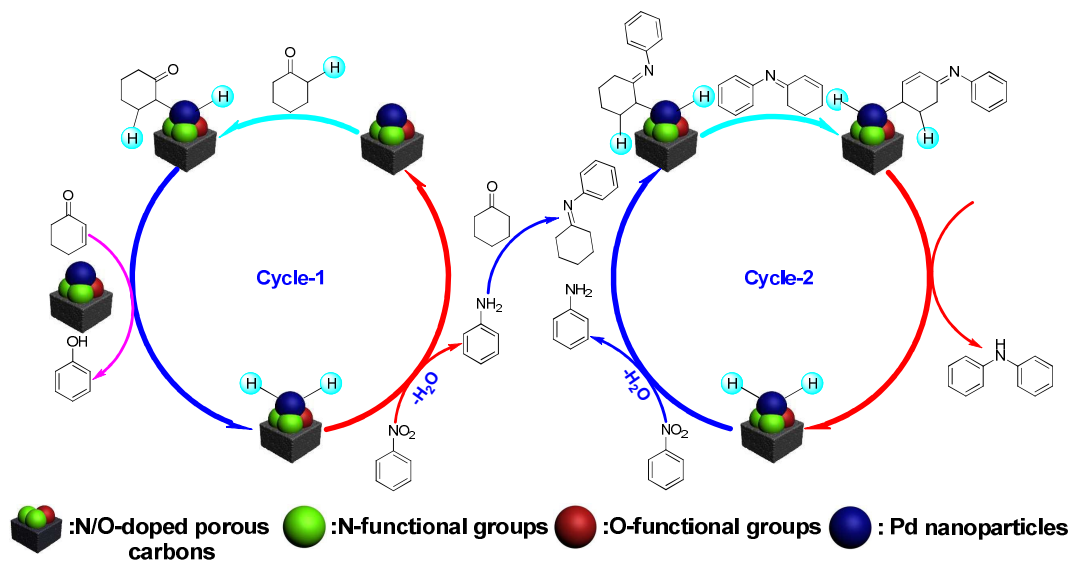


Entry	t/h	Con.% ^b	Y (B).% ^c	Y (C).% ^c
1	0.5	20	6	13
2	1	99	31	64
3	2	99	31	63
4	4	99	32	66

^a0.5 mmol N-cyclohexylideneaniline, 30 mg Pd/C-py, 5 mL toluene, 160 °C (reaction temperature), Ar. ^bConversion of N-cyclohexylideneaniline determined by GC-FID with external standard method. ^cGC yields.

Following, we verified the role of N-cyclohexylideneaniline in the reaction, so it was used as the starting material directly with Pd/C-py as catalyst (**Table 4**). Obviously, N-cyclohexylideneaniline can be converted into diphenylamine and N-cyclohexylaniline in 1 h. Noteworthy, the reaction finished in 1 h and then the yields of diphenylamine and N-cyclohexylaniline maintained stable (**Table 4, entries 2-4**). That signifies N-cyclohexylideneaniline can be converted into the desired product very fast and N-cyclohexylideneaniline might be the key intermediate.

Based on these results, a possible reaction mechanism is proposed (**Scheme 7**). For the dehydrogenation of cyclohexanone to 2-cyclohexen-1-one in the reaction process-A, deprotonative coordination of cyclohexanone to Pd with the assistance of N/O-doped porous carbons affords Pd-enolate-H species, followed by β -H elimination to give 2-cyclohexen-1-one. Then the catalytic dehydrogenation of 2-cyclohexen-1-one to phenol occurred through a catalytic cycle (cycle-1), which was similar to the dehydrogenation of cyclohexanone to 2-cyclohexen-1-one. Meanwhile, the catalytic hydrogenation of a small amount of nitrobenzene to aniline by Pd-2H can then regenerate the catalyst. The aniline generated during reaction-A will react with cyclohexanone quickly and generate N-cyclohexylideneaniline. Then, reaction-B were happened between N-cyclohexylideneaniline and nitrobenzene to give diphenylamine as product with the concomitant formation of the Pd-2H species. The Pd-2H species and nitrobenzene would continue the reaction, and the active catalyst would be regenerated for the next cycle (cycle-2).



Scheme 7. Proposed reaction mechanism.

4. CONCLUSIONS

In summary, we have developed a general method for the precise construction and functionalization of porous carbon materials with tunable N/O functional groups via pyrrole/furan polymerization and pyrolyzation. These N/O doped carbons can behave as support and "solid ligand" to

immobilize nanopalladium, which can be an active catalyst for biphenylamine and triphenylamine synthesis through the reaction of nitrobenzene and cyclohexanone. The catalytic performance can be tuned efficiently via tuning the N/O group contents and ratios on the carbon material surface,

Journal Name

ARTICLE

which can coordinate with the Pd nanoparticles to modulate the size and electronic properties of Pd nanoparticles via the electron-donating from Pd nanoparticles to the N/O species. In addition, mechanistic studies prove that this reaction starts with the transferhydrogenation reaction between nitrobenzene and cyclohexanone to generate aniline. Then aniline would react with cyclohexanone to form N-cyclohexylideneaniline, and biphenylamine could be synthesized through its further reaction with nitrobenzene. This work should open up a promising pathway for the development of new method for arylamine synthesis, and structure and activity defined heterogeneous catalysts for fine chemical synthesis.

Acknowledgements

This work was financially supported by the National Natural Science Foundation of China (21633013) and Youth Innovation Promotion Association CAS.

References

- J. Greeley, J. K. Nørskov and M. Mavrikakis, *Annu. Rev. Phys. Chem.*, 2002, **53**, 319-348.
- T. D. Tilley, *J. Mol. Catal. A: Chem.*, 2002, **182**, 17-24.
- D. K. Böhme and H. Schwarz, *Angew. Chem. Int. Ed.*, 2005, **44**, 2336-2354.
- P. Mäki-Arvela, J. Hajek, T. Salmi and D. Y. Murzin, *Appl. Catal., A*, 2005, **292**, 1-49.
- P. V. Kamat, *J. Phys. Chem. C*, 2007, **111**, 2834-2860.
- G. A. Somorjai and J. Y. Park, *Angew. Chem. Int. Ed.*, 2008, **47**, 9212-9228.
- V. Dal Santo, F. Liguori, C. Pirovano and M. Guidotti, *Molecules*, 2010, **15**, 3829-3856.
- H. Dau, C. Limberg, T. Reier, M. Risch, S. Roggan and P. Strasser, *ChemCatChem*, 2010, **2**, 724-761.
- E. A. Quadrelli and J.-M. Basset, *Coord. Chem. Rev.*, 2010, **254**, 707-728.
- D. Gajan, G. Lapadula, M. Schwarzwälder and C. Copéret, *Spectroscopic Properties of Inorganic and Organometallic Compounds*, ed. J. Yarwood, R. Douthwaite and S. Duckett, *Royal Society of Chemistry*, 2012, **43**, 57.
- R. Cheng, Z. Liu, L. Zhong, X. He, P. Qiu, M. Terano, M. S. Eisen, S. L. Scott and B. Liu, in *Polyolefins: 50 years after Ziegler and Natta I*, Springer, 2013, pp. 135-202.
- D. Haag and H. H. Kung, *Top. Catal.*, 2014, **57**, 762-773.
- X.-K. Kong, C.-L. Chen and Q.-W. Chen, *Chem. Soc. Rev.*, 2014, **43**, 2841-2857.
- C. J. Shearer, A. Cherevan and D. Eder, *Adv. Mater.*, 2014, **26**, 2295-2318.
- X. Duan, Z. Ao, H. Sun, S. Indrawirawan, Y. Wang, J. Kang, F. Liang, Z. H. Zhu and S. Wang, *ACS Appl. Mat. Interfaces*, 2015, **7**, 4169-4178.
- H. Yang, X. Cui, X. Dai, Y. Deng and F. Shi, *Nat. Commun.*, 2015, **6**.
- D. R. Dreyer, H. P. Jia and C. W. Bielawski, *Angew. Chem. Int. Ed.*, 2010, **49**, 6813-6816.
- B. Frank, M. Morassutto, R. Schomäcker, R. Schlögl and D. S. Su, *ChemCatChem*, 2010, **2**, 644-648.
- J. McGregor, Z. Huang, E. P. Parrott, J. A. Zeitler, K. L. Nguyen, J. M. Rawson, A. Carley, T. W. Hansen, J.-P. Tessonnier and D. S. Su, *J. Catal.*, 2010, **269**, 329-339.
- A. Rinaldi, J. Zhang, B. Frank, D. S. Su, S. B. Abd Hamid and R. Schlögl, *ChemSusChem*, 2010, **3**, 254-260.
- H. Chen, M. He, Y. Wang, L. Zhai, Y. Cui, Y. Li, Y. Li, H. Zhou, X. Hong and Z. Deng, *Green Chem.*, 2011, **13**, 2723-2726.
- D. R. Dreyer, H.-P. Jia, A. D. Todd, J. Geng and C. W. Bielawski, *Org. Biomol. Chem.*, 2011, **9**, 7292-7295.
- H. Huang, J. Huang, Y.-M. Liu, H.-Y. He, Y. Cao and K.-N. Fan, *Green Chem.*, 2012, **14**, 930-934.
- Y. Chen, J. Zhang, M. Zhang and X. Wang, *Chem. Sci.*, 2013, **4**, 3244-3248.
- P. Zhang, Y. Gong, H. Li, Z. Chen and Y. Wang, *Nat. Commun.*, 2013, **4**, 1593.
- T. N. Hoheisel, S. Schrettl, R. Szilluweit and H. Frauenrath, *Angew. Chem. Int. Ed.*, 2010, **49**, 6496-6515.
- D. Quiñero, A. Frontera and P. M. Deyà, *J. Phys. Chem. C*, 2012, **116**, 21083-21092.
- Z. k. Sofer, O. e. Jankovský, P. Šimek, D. Sedmidubský, J. i. Šturala, J. i. Kosina, R. Mikšová, A. Macková, M. Mikulics and M. Pumera, *ACS Nano*, 2015, **9**, 5478-5485.
- K. Shen, X. Chen, J. Chen and Y. Li, *ACS Catal.*, 2016, **6**, 5887-5903.
- K. Yuan, T. Hu, Y. Xu, R. Graf, G. Bruncklaus, M. Forster, Y. Chen and U. Scherf, *ChemElectroChem*, 2016, **3**, 822-828.
- C. E. Davies, I. M. Gardiner, J. C. Green, M. L. Green, N. J. Hazel, P. D. Grebenik, V. S. Mtetwa and K. Prout, *J. Chem. Soc., Dalton Trans.*, 1985, 669-683.
- R. S. Tanke and R. H. Crabtree, *J. Am. Chem. Soc.*, 1990, **112**, 7984-7989.
- S. Gorelsky, E. Dodsworth, A. Lever and A. Vlcek, *Coord. Chem. Rev.*, 1998, **174**, 469-494.
- C. Pettinari, M. Pellei, M. Miliani, A. Cingolani, A. Cassetta, L. Barba, A. Pifferi and E. Rivarola, *J. Organomet. Chem.*, 1998, **553**, 345-369.
- P. Lightfoot and A. Snedden, *J. Chem. Soc., Dalton Trans.*, 1999, 3549-3551.
- A. Chakravorty, *Eur. J. Inorg. Chem.*, 2005, **2005**, 4863-4874.
- H. Fleischer, *Coord. Chem. Rev.*, 2005, **249**, 799-827.
- Y. Zhou, M. Hong and X. Wu, *Chem. Commun.*, 2006, 135-143.

39. J. T. York, I. Bar-Nahum and W. B. Tolman, *Inorg. Chim. Acta*, 2008, **361**, 885-893.
40. G.-X. Liu, K. Zhu, H.-M. Xu, S. Nishihara, R.-Y. Huang and X.-M. Ren, *CrystEngComm*, 2009, **11**, 2784-2796.
41. F. Fache, E. Schulz, M. L. Tommasino and M. Lemaire, *Chem. Rev.*, 2000, **100**, 2159-2232.
42. Z. Wang, K. Ding and Y. Uozumi, *Handbook of Asymmetric Heterogeneous Catalysis*, 2008.
43. M. K. Lam, K. T. Lee and A. R. Mohamed, *Biotechnol. Adv.*, 2010, **28**, 500-518.
44. R. A. Shiels and C. W. Jones, in *Model Systems in Catalysis*, Springer, 2010, pp. 441-455.
45. C. A. Witham, W. Huang, C.-K. Tsung, J. N. Kuhn, G. A. Somorjai and F. D. Toste, *Nat. Chem.*, 2010, **2**, 36-41.
46. S. S. Zaleskiy, A. E. Sedykh, A. S. Kashin and V. P. Ananikov, *J. Am. Chem. Soc.*, 2013, **135**, 3550-3559.
47. S. B. Singh and P. K. Tandon, *J. ENERGY*, 2014, **2**, 106-115.
48. R. Cano, A. F. Schmidt and G. P. McGlacken, *Chem. Sci.*, 2015, **6**, 5338-5346.
49. G. Odian, *Principles of polymerization*, John Wiley & Sons, 2004.
50. D. Wang, N. L. Smith and P. M. Budd, *Polym. Int.*, 2005, **54**, 297-303.
51. T. Kowalewski, T. CHUANBING, M. Kruk, B. Dufour and K. Matyjaszewski, In *Advances in nanostructured carbons from block copolymers prepared by controlled radical polymerization techniques*, ACS Symp. Ser., Oxford University Press: 2006; pp 295-310.
52. J. T. McCann, B. Lim, R. Ostermann, M. Rycenga, M. Marquez and Y. Xia, *Nano Lett.*, 2007, **7**, 2470-2474.
53. L. Luo, C. Wilhelm, C. N. Young, C. P. Grey, G. P. Halada, K. Xiao, I. N. Ivanov, J. Y. Howe, D. B. Geohegan and N. S. Goroff, *Macromolecules*, 2011, **44**, 2626-2631.
54. S. Zhu, Q. Meng, L. Wang, J. Zhang, Y. Song, H. Jin, K. Zhang, H. Sun, H. Wang and B. Yang, *Angew. Chem. Int. Ed.*, 2013, **52**, 3953-3957.
55. Y.-W. Zeng, D.-K. Ma, W. Wang, J.-J. Chen, L. Zhou, Y.-Z. Zheng, K. Yu and S.-M. Huang, *Appl. Surf. Sci.*, 2015, **342**, 136-143.
56. M. Duan, Y.-m. Tian and S.-z. Li, *New Carbon Mater.*, 2016, **31**, 62-67.
57. R. B. Gennis, *Biomembranes: molecular structure and function*, Springer Science & Business Media, 2013.
58. M. Marguet, C. Bonduelle and S. Lecommandoux, *Chem. Soc. Rev.*, 2013, **42**, 512-529.
59. C. Zeng, T. Li, A. Das, N. L. Rosi and R. Jin, *J. Am. Chem. Soc.*, 2013, **135**, 10011-10013.
60. A. Laganowsky, E. Reading, T. M. Allison, M. B. Ulmschneider, M. T. Degiacomi, A. J. Baldwin and C. V. Robinson, *Nature*, 2014, **510**, 172.
61. Q.-A. Chen, Z.-S. Ye, Y. Duan and Y.-G. Zhou, *Chem. Soc. Rev.*, 2013, **42**, 497-511.
62. T. Hattori, A. Tsubone, Y. Sawama, Y. Monguchi and H. Sajiki, *Tetrahedron*, 2014, **70**, 4790-4798.
63. Y. Chen, J. P. Romaine and T. R. Newhouse, *J. Am. Chem. Soc.*, 2015, **137**, 5875-5878.
64. A. V. Iosub and S. S. Stahl, *J. Am. Chem. Soc.*, 2015, **137**, 3454-3457.
65. I. Shin, S. D. Ramgren and M. J. Krische, *Tetrahedron*, 2015, **71**, 5776-5780.
66. Y. Chen, A. Turlik and T. Newhouse, *Synfacts*, 2016, **12**, 0370-0370.
67. S. P. Cummings, T. N. Le, G. E. Fernandez, L. G. Quiambao and B. J. Stokes, *J. Am. Chem. Soc.*, 2016.
68. A. V. Iosub and S. S. Stahl, *ACS Catal.*, 2016.
69. P. J. Das, Y. Diskin-Posner, M. Firer, M. Montag and F. Grynszpan, *Dalton Trans.*, 2016, **45**, 17123-17131.
70. J. Zhao, Z. Li, S. Song, M. A. Wang, B. Fu and Z. Zhang, *Angew. Chem. Int. Ed.*, 2016, **55**, 5545-5549.
71. A. B. Fuertes and T. A. Centeno, *J. Mater. Chem.*, 2005, **15**, 1079-1083.
72. C.-M. Yang, C. Weidenthaler, B. Spliethoff, M. Mayanna and F. Schüth, *Chem. Mater.*, 2005, **17**, 355-358.
73. M. Lezanska, P. Pietrzyk and Z. Sojka, *J. Phys. Chem. C*, 2009, **114**, 1208-1216.
74. M. Sevilla, P. Valle-Vigón and A. B. Fuertes, *Adv. Funct. Mater.*, 2011, **21**, 2781-2787.
75. A. Bakhshi, J. Ladik and M. Seel, *Phys. Rev. B*, 1987, **35**, 704.
76. D. Wang, Y.-X. Li, Z. Shi, H.-L. Qin, L. Wang, X.-F. Pei and J. Jin, *Langmuir*, 2010, **26**, 14405-14408.
77. L. Cui, J. Shen, F. Cheng, Z. Tao and J. Chen, *J. Power Sources*, 2011, **196**, 2195-2201.
78. P. Jha, S. P. Koiry, V. Saxena, P. Veerender, A. K. Chauhan, D. K. Aswal and S. K. Gupta, *Macromolecules*, 2011, **44**, 4583-4585.
79. S. Zhen, J. Xu, B. Lu, S. Zhang, L. Zhao and J. Li, *Electrochim. Acta*, 2014, **146**, 666-678.
80. A. S. Guram, R. A. Rennels and S. L. Buchwald, *Angew. Chem. Int. Ed.*, 1995, **34**, 1348-1350.
81. D. B. Ramachary, K. Ramakumar and V. V. Narayana, *J. Org. Chem.*, 2007, **72**, 1458-1463.
82. G. P. López, D. G. Castner and B. D. Ratner, *Surf. Interface Anal.*, 1991, **17**, 267-272.
83. T. Tokushima, Y. Horikawa, Y. Harada, O. Takahashi, A. Hiraya and S. Shin, *PCCP*, 2009, **11**, 1679-1682.
84. L.-Z. Fan, S. Qiao, W. Song, M. Wu, X. He and X. Qu, *Electrochim. Acta*, 2013, **105**, 299-304.
85. H. Liu, Y. Zhang, R. Li, X. Sun, S. Désilets, H. Abou-Rachid, M. Jaidann and L.-S. Lussier, *Carbon*, 2010, **48**, 1498-1507.
86. S. Martha, A. Nashim and K. Parida, *J. Mater. Chem. A*, 2013, **1**, 7816-7824.
87. H. Xu, J. Yan, Y. Xu, Y. Song, H. Li, J. Xia, C. Huang and H. Wan, *Appl. Catal., B*, 2013, **129**, 182-193.
88. G. Mestl, N. I. Maksimova, N. Keller, V. V. Roddatis and R. Schlögl, *Angew. Chem. Int. Ed.*, 2001, **40**, 2066-2068.
89. N. Keller, N. I. Maksimova, V. V. Roddatis, M. Schur, G. Mestl, Y. V. Butenko, V. L. Kuznetsov and R. Schlögl, *Angew. Chem. Int. Ed.*, 2002, **41**, 1885-1888.
90. V. Strelko, N. Kartel, I. Dukhno, V. Kuts, R. Clarkson and B. Odintsov, *Surf. Sci.*, 2004, **548**, 281-290.
91. J. Zhang, X. Liu, R. Blume, A. Zhang, R. Schlögl and D. S. Su, *Science*, 2008, **322**, 73-77.
92. C. Chen, J. Zhang, B. Zhang, C. Yu, F. Peng and D. Su, *Chem. Commun.*, 2013, **49**, 8151-8153.
93. X. Cui, Y. Li, S. Bachmann, M. Scalone, A.-E. Surkus, K. Junge, C. Topf and M. Beller, *J. Am. Chem. Soc.*, 2015, **137**, 10652-10658.
94. W. Shi, B. Zhang, Y. Lin, Q. Wang, Q. Zhang and D. S. Su, *ACS Catal.*, 2016, **6**, 7844-7854.

95. O. E. Andersson, B. Prasad, H. Sato, T. Enoki, Y. Hishiyama, Y. Kaburagi, M. Yoshikawa and S. Bandow, *Phys. Rev. B*, 1998, **58**, 16387.
96. D. Klein and L. Bytautas, *J. Phys. Chem. A*, 1999, **103**, 5196-5210.
97. G. Zhou, W. Duan and B. Gu, *Chem. Phys. Lett.*, 2001, **333**, 344-349.
98. W. L. Mao, H.-k. Mao, P. J. Eng, T. P. Trainor, M. Newville, C.-c. Kao, D. L. Heinz, J. Shu, Y. Meng and R. J. Hemley, *Science*, 2003, **302**, 425-427.
99. J. Lu, J.-x. Yang, J. Wang, A. Lim, S. Wang and K. P. Loh, *ACS Nano*, 2009, **3**, 2367-2375.
100. L. Mazalov, S. Trubina, N. Kryuchkova, O. Tarasenko, S. Trubin and G. Zharkova, *J. Struct. Chem.*, 2007, **48**, 253-261.
101. J. H. Shim, X. Jiang, S. F. Bent and F. B. Prinz, *J. Electrochem. Soc.*, 2010, **157**, B793-B797.
102. Y. Kee, S. Esa, B. Rahim and W. Ismail, In *Surface elemental quantification of Au-Pd pre-plated leadframe by means of X-ray Photoelectron Spectroscopy*, Physical and Failure Analysis of Integrated Circuits (IPFA), 2016 IEEE 23rd International Symposium on the, IEEE: 2016; pp 136-139.
103. Y. Zhang, Z. Yuan and R. J. Puddephatt, *Chem. Mater.*, 1998, **10**, 2293-2300.
104. X. Luo, W. Huang, Y. Mei, S. Zhou and L. Zhu, *Inorg. Chem.*, 1999, **38**, 1474-1480.
105. Y.-L. Tung, W.-C. Tseng, C.-Y. Lee, P.-F. Hsu, Y. Chi, S.-M. Peng and G.-H. Lee, *Organometallics*, 1999, **18**, 864-869.
106. J.-W. Park, Y.-M. Chung, Y.-W. Suh and H.-K. Rhee, *Catal. Today*, 2004, **93**, 445-450.
107. O. Beyssac, B. Goffé, J.-P. Petitot, E. Froigneux, M. Moreau and J.-N. Rouzaud, *Spectrochim. Acta, Part A*, 2003, **59**, 2267-2276.
108. C. Shan, H. Yang, D. Han, Q. Zhang, A. Ivaska and L. Niu, *Langmuir*, 2009, **25**, 12030-12033.
109. I.-Y. Jeon, H.-J. Choi, M. J. Ju, I. T. Choi, K. Lim, J. Ko, H. K. Kim, J. C. Kim, J.-J. Lee and D. Shin, *Sci. Rep.*, 2013, **3**.
110. B. Guo, Q. Liu, E. Chen, H. Zhu, L. Fang and J. R. Gong, *Nano Lett.*, 2010, **10**, 4975-4980.
111. V. Georgakilas, M. Otyepka, A. B. Bourlinos, V. Chandra, N. Kim, K. C. Kemp, P. Hobza, R. Zboril and K. S. Kim, *Chem. Rev.*, 2012, **112**, 6156-6214.
112. K. Taniguchi, X. Jin, K. Yamaguchi and N. Mizuno, *Catal. Sci. Technol.*, 2016, **6**, 3929-3937.
113. Y. Xie, S. Liu, Y. Liu, Y. Wen and G.-J. Deng, *Org. Lett.*, 2012, **14**, 1692-1695.
114. M. Sutter, M.-C. Duclos, B. Guicharet, Y. Raoul, E. Métay and M. Lemaire, *ACS Sustainable Chem. Eng.*, 2013, **1**, 1463-1473.
115. S. A. Girard, X. Hu, T. Knauber, F. Zhou, M.-O. Simon, G.-J. Deng and C.-J. Li, *Org. Lett.*, 2012, **14**, 5606-5609.
116. A. Hajra, Y. Wei and N. Yoshikai, *Org. Lett.*, 2012, **14**, 5488-5491.
117. R. Bautista, P. A. Montoya, A. Rebollar, E. Burgueño and J. Tamariz, *Molecules*, 2013, **18**, 10334-10351.
118. J. Zhang, Q. Jiang, D. Yang, X. Zhao, Y. Dong and R. Liu, *Chem. Sci.*, 2015, **6**, 4674-4680.

